RSC Advances

PAPER

View Article Online
View Journal | View Issue

Cite this: *RSC Adv.*, 2024, **14**, 954

Nanoclay-reinforced alginate aerogels: preparation and properties†

Bang-Ting Xu, [a] Da-zhi Jin,*[ab] Yi Yu,[a] Qi Zhang,[a] Weng-jie Weng,[a] Kai-xiang Ren[a] and Yu-Lei Tai*[ab]

Flame-retardant materials that are mechanically robust, low cost and non-toxic from green and renewable resources are highly demanded in many fields. In this work, aerogels of alginate extracted from seaweeds were fabricated and reinforced with nanoclay. The nanoclay particles increase the molecular ordering (crystallinity) of the aerogels through physical interactions with alginate molecules. They also served as cross-linkers and flame-retardant additives to improve the mechanical strength, elasticity, thermal stability and flame-retarding properties of the aerogels. Under exposure to a butane flame (750 °C), the aerogels maintained their structural integrity and did not produce drips. An optimal loading of nanoclay which led to the best flame retardancy (non-flammable) of the aerogel was determined. The results of this work demonstrate that alginate-nanoclay composite aerogels can be promisingly used as flame-retardant thermal insulation materials.

Received 19th October 2023
Accepted 11th December 2023

DOI: 10.1039/d3ra07132d

rsc.li/rsc-advances

1 Introduction

With growing awareness in environmental protection and hazard prevention, thermal insulating materials that are green and with low flammability are increasingly demanded in many fields such as construction, automotive and aerospace. The current market of thermal insulation materials is dominated by those made of synthetic organic compounds. Among these materials, polymeric foams, especially, polystyrene and polyurethane foams are the most common.[1,2] However, polymeric foams have many limitations including low oxygen indexes and inherently low flame resistance. Usually, these materials are almost exclusively petroleum-based, which are highly flammable and generate toxic gases when they burn. Their burning often results in the formation of low-viscous tars that can drip to cause secondary fires. The release of toxic gases is also detrimental during a fire accident.[3,4] To enhance their fire-resistance, flame retardants are generally incorporated into these materials. Unfortunately, many of the flame retardants not only make the disposal and recycling of the materials difficult, but also make fires more deadly.[5,6] Hence, developing thermal insulation materials that are non-toxic, biodegradable with low flammability and low thermal conductivity from natural and renewable resources is attractive and worth efforts.[7,8] Nevertheless, the materials shall also have sufficient mechanical properties.

Among all the natural materials for thermal insulation applications, the most interesting is alginate, which could be easily extracted from an abundant resource, seaweeds, using simple and green chemical processes.[9] Alginate is a type of polysaccharide composed of β-(1 → 4)-D-mannuronic and α-L-guluronic acid blocks in heterogeneous proportions. It is mainly found in the cellular wall matrix of brown seaweeds (Phaeophyceae), in the form of an insoluble calcium or magnesium salt.[10] Alginate is a polyelectrolyte as well, which possess a high selectivity to alkaline metal ions and binds Ca^{2+} ion resulting in gel formation. This binding capacity of alginate is attributable to its two α-L-guluronic acid blocks. This low-cost natural biomaterial possesses excellent properties, for example, excellent biocompatibility and biodegradability, hydrophilicity, gel-forming abilities, salt-tolerant and underwater superoleophobic properties, *etc*[11]. These properties have contributed to the applications of alginate-based materials in areas such as environmental protection,[10] agriculture,[12] biomedical engineering,[13–15] thermal insulation/fire retarding[16,17] and so on. Same to aerogels of other materials, an alginate aerogel has a porous structure, which make it lightweight and suitable to thermal insulation. However, alginate aerogels are fragile and lack sufficient mechanical strength, which limit their applications.[18]

Composite formation using nanofiller/crosslinkers has been widely adopted to produce mechanically robust materials.[19–21] In the context of thermal insulation, the nanofiller shall not only improve the mechanical properties of a material but also have inherently low flammability.[22] Clay is one of the most

[a]*School Laboratory of Medicine, Hangzhou Medical College, Hangzhou, Zhejiang, 310053, P. R. China. E-mail: jind@hmc.edu.cn; taiyulei@hmc.edu.cn*

[b]*Laboratory of Biomarkers and* In Vitro *Diagnosis Translation of Zhejiang Province, Hangzhou Medical College, Hangzhou, Zhejiang, 310053, P. R. China*

† Electronic supplementary information (ESI) available. See DOI: https://doi.org/10.1039/d3ra07132d

widely used inorganic flame-retarding additives for its excellent properties such as tastelessness, non-toxicity, heat and flame resistance, and non-volatility.[18,23,24] Hydrophilic bentonite, montmorillonite clay, is composed of tetrahedral silica sheets layered between alumina octahedral sheets.[25] Its imperfect crystal lattice and the isomorphic substitution induce a net negative charge, which benefits the adsorption of alkaline earth metal ions in the interlayer space and contribute to the activity and reactions/interactions with polymers.[25] The montmorillonite clay also possesses excellent reactivity due to the dangling hydroxyl end-groups on its surfaces, and has large specific surface area, good mechanical strength, which enables the formation of polymer composites with significantly improved mechanical properties.[26] Hence, montmorillonite nanoclay shall be an excellent additive to reinforce alginate aerogels and improve their flame retarding property.

Herein, in this work, we report the fabrication of low-cost and robust alginate-nanoclay hybrid aerogels with excellent flame retarding properties by a facile method combing freeze-drying and ionic cross-linking. The effects of nanoclay content, sodium alginate content and moisture content on the mechanical properties and flame resistance of the aerogels are investigated. The aerogels demonstrate a great potential for flame-retarding applications. In addition, as alginate could be easily processed into various forms including hydrogels, aerogels, beads, films and fibers with a great flexibility in shape and size,[19] this work will inspire the fabrication of a range of alginate-nanoclay composites that integrates the merits of these two components for different applications.

2 Experimental

2.1 Materials

Hydrophilic bentonite (nanoclay, montmorillonite clay, nanomer) was purchased from Sigma-Aldrich. Seaweed Sargassum muticum was collected from the coastal area of Geelong, Australia, and stored in a freezer (−20 °C) until use. All chemicals used in this work are of analytical grade and were used as received without any further purification.

2.2 Fabrication of alginate-nanoclay aerogels

2.2.1 Extraction of alginate from sargassum muticum seaweeds. Seaweeds were firstly dried in an oven at 65 °C until a constant weight was reached. Dry seaweeds (20 g) were soaked in 200 mL of 0.2% formaldehyde for 24 h at room temperature to remove the coloured pigments present in the cell wall, followed by washing with Milli-Q water. Then, 200 mL of 0.2 M HCl was added to turn the insoluble alginic salts to alginic acid. Acidified seaweeds were thoroughly washed with Milli-Q water before a solution of sodium carbonate (3%, pH 12) was added. They were then incubated at 90 °C for 3 h. The insoluble fraction was collected by centrifugation at 10 000×*g*, and the sodium alginate dissolved in the supernatant was precipitated with aqueous ethanol (90%). The precipitated mass was collected and dissolved in 200 mL of Milli-Q water and shaken overnight at 100 rpm. Finally, the dissolved sodium alginate was precipitated using aqueous ethanol, collected on filter papers and dried at 65 °C.[27]

2.2.2 Preparation of alginate-nanoclay aerogels. The typical procedure to prepare the aerogels is described as followed: firstly, weighed amounts of nanoclay were slowly dispersed into each of 12 mL of 2% alginate aqueous solutions with continuous stirring to produce homogeneous gels, resulting in nanoclay concentrations of 0.08%, 0.24%, 0.40%, 0.64%, 0.89% and 1.06%. The gels were poured into a mold and frozen in a freezer. The frozen samples were then freeze-dried in a benchtop freeze dryer (Labconco, USA) at −85 °C for 48 h. The gels were immersed in a saturated calcium chloride–ethanol solution at room temperature for 8 h to ensure complete cross linking of alginate. Then the gels were washed with ethanol three times to remove residual calcium chloride and dried in vacuum oven at 40 °C for 8 h to eliminate ethanol. The aerogels containing the different amounts of nanoclays were named as AC-1, AC-2, AC-3, AC-4, AC-5 and AC-6, respectively. An aerogel without nanoclay was also prepared and named as SA.

2.3 Characterizations

2.3.1 Morphology and structure of aerogels. The morphology of aerogels was observed with Supra Zeiss 55VP field emission scanning electron microscopy (SEM) at an accelerated voltage of 5 kV.

FT-IR analysis was performed on a Bruker vertex 70 FTIR spectrometer in the attachment total reflection (ATR) mode to observe the structure and chemical bonds in the wavenumber range of 500–4000 cm^{-1}.

The crystal structures of aerogels were analyzed with an X-ray diffractometer (XRD), using an X-pert Power with Cu kα radiation generated at 40 kV and 20 mA. The scanning rate was 4°·min^{-1} over a range of 5°–80°.

2.3.2 Mechanical properties of aerogels. The mechanical properties (compression elastic modulus) of the as-synthesized aerogels were characterized at 25 °C using a universal test machine (Instron 30KN tensile tester) with a 1 KN load cell. All aerogels were cut into cylinders (12 mm in diameter and 12 mm in height) and compressed at a loading rate of 2 mm × min^{-1} for strain cycles. Loading and unloading curves with compressive strains of 10%, 20%, 40% and 60% were recorded. The mechanical properties (compression elastic modulus) of the as-synthesized aerogels were characterized at 25 °C using a universal test machine (Instron 30KN tensile tester) with a 1 KN load cell. All aerogels were cut into cylinders (12 mm in diameter and 12 mm in height) and compressed at a loading rate of 2 mm × min^{-1} for strain cycles. Loading and unloading curves with compressive strains of 10%, 20%, 40% and 60% were recorded.

2.3.3 Thermal and anti-flame properties of aerogels. Thermal analysis was performed with a thermogravimetric analyzer (TGA) Q50 from room temperature to 800 °C at a heating rate of 20 °C min^{-1} under an argon and air atmosphere, respectively. The moisture contents of aerogels were also measured by the TGA analyzer from room temperature to 200 °C at a heating rate of 5 °C min^{-1} under an argon

atmosphere. The porosity and BET surface area of sample AC 4 was measured using N_2 physio-sorption analysis at 150 °C on a Micromeritics ASPS 2010 analyzer and sample was pre-treated at 100 °C under vacuum for 24 h.

The capability of as-prepared SA aerogels and AC aerogels to resist flame penetration was evaluated under a simulated ignition event. Briefly, the centers of the top surface of the aerogels (cylindrical shape) were exposed to a butane flame from a distance of *c.a.* 100 mm resulting in a temperature of 750 °C on the exposed surface. The flame was applied continuously until the sample is penetrated or up to 180 s, observed with a camera. The residues of aerogels were obtained by calculating the weight ratio of samples before and after burning tests.

3 Results and discussion

3.1 Morphology and structure of AC aerogels

Fig. 1 shows the SEM images of the aerogels without and with nanoclays. All the aerogels possess cellular porous microstructures, which except that of AC-6 show an obvious orientation. The structural orientation shall be induced by the temperature gradient through the solutions during freezing drying. Orientated structures are frequent for aerogels/scaffolds of different polymers prepared by freeze drying.[28,29] The formation of non-orientated structure in AC-6 could be due to its high nanoclay loading, which has a big effect on the nucleation and crystallization of alginate. Like other crystallization systems, the crystallization of alginate in this work is governed by thermodynamics and kinetics. While thermodynamics is controlled by the degree of supercooling or supersaturation, kinetics is affected by the presence of additives/impurities.[30,31] Nanoclay particles which have multiple interactions with alginate molecules (to be discussed later) can affect the nucleation and crystallization of alginate. The kinetic effect is more obvious at a higher nanoclay concentration. When the concentration of nanoclay in high enough, the effects of thermodynamics are offset, and temperature-gradient-induced structural orientation is not obvious. In addition, the structure of aerogel becomes denser with an increase in nanoclay concentration, which is particularly obvious for AC-5 and AC-6 having nanoclay at the concentrations of 0.89% and 1.06%, respectively.

The XRD spectra of aerogels (SA and AC) and nanoclay are presented in Fig. 2a. With the addition of nanoclay, the peaks of aerogels at 38.2°, 44.6°, 65.1° and 78.4° did not change, but the diffraction peak of nanoclay itself at 19.9°, 35.9° and 61.7°

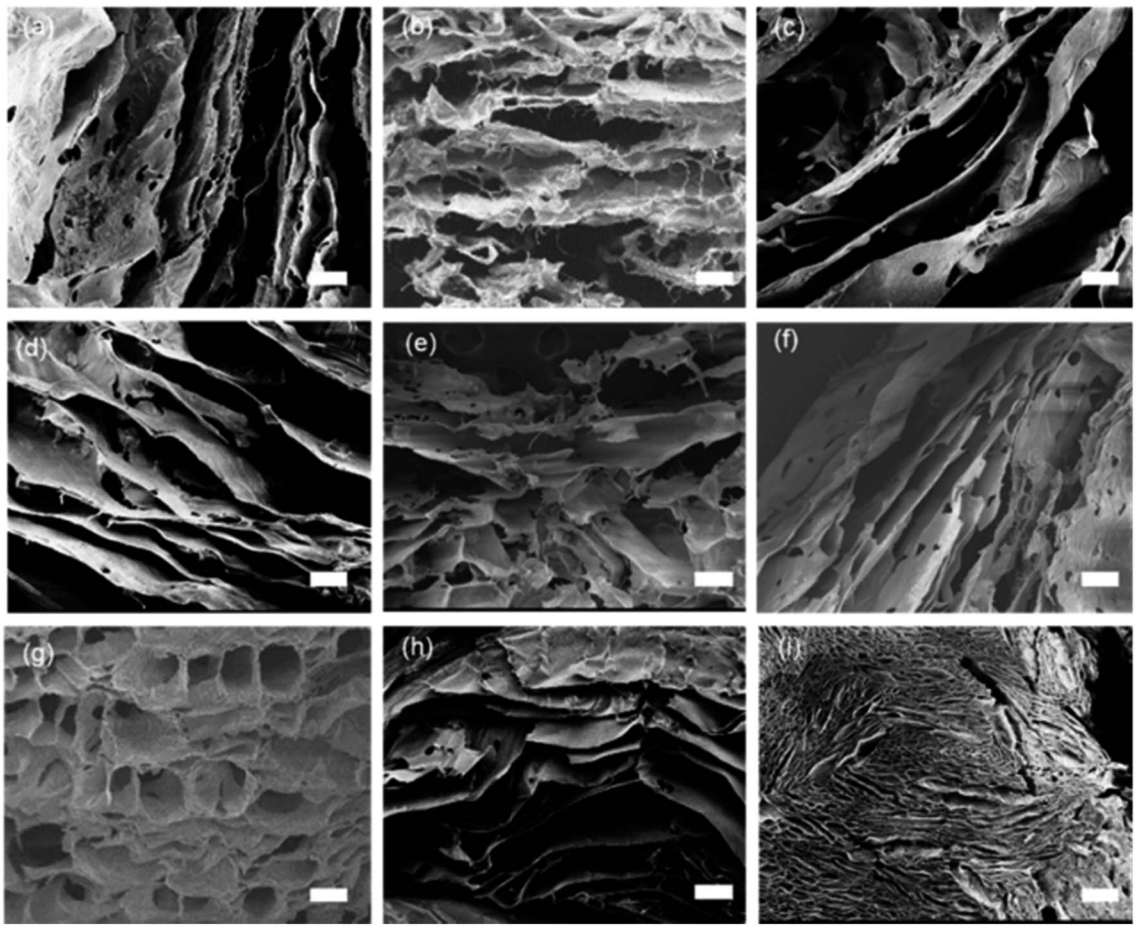

Fig. 1 SEM images of SA and AC aerogels. (a) SA aerogel, (b) AC-1, (c) AC-2, (d) AC-3, (e) AC-4, (f) AC-5, (g) AC-6, (h) AC aerogel with 3% sodium alginate and 0.64% nanoclay, and (i) AC aerogel with 4.5% sodium alginate and 0.64% nanoclay. The scale bars represent 200 nm.

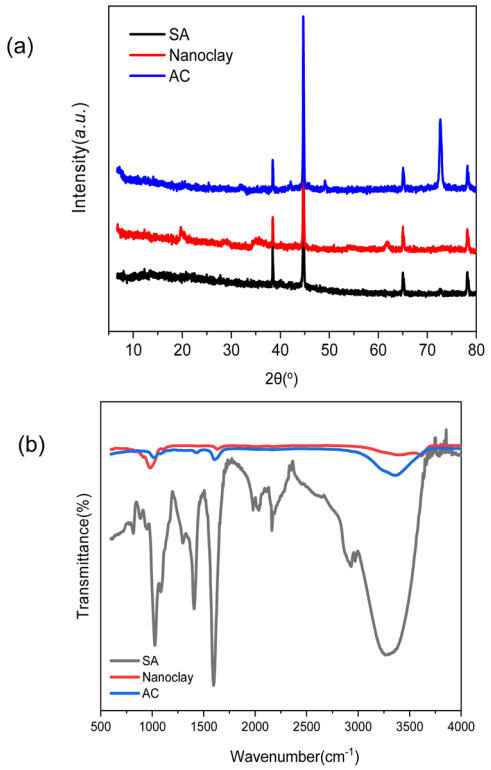

Fig. 2 XRD and FT-IR spectra of pure nanoclay, sodium alginate aerogels and alginate-nanoclay aerogel (AC-4). (a) XRD and (b) FT-IR spectra.

became less sharp. The peak at 72.8° of the aerogels is significantly enhanced. The results indicate that nanoclay has no effect on crystal structure of the alginate aerogels. This is in agreement with the FTIR results that alginate was not intercalated into the mineral structure of nanoclay and no covalent interactions occurred between them. Instead, alginate should interact with the surface hydroxyl groups of nanoclay merely through electrostatic and hydrogen bonds.

To elucidate the changes in functional groups of alginate after encapsulating nanoclay in aerogels, FT-IR analysis was carried out (Fig. 2b). In the spectrum of pure nanoclay, vibration at 3400 and 3625 cm^{-1} corresponds to the –OH stretching mode in Si–OH and Al–OH bonds, respectively.[32] The bending vibration of water appeared at 1630 cm^{-1} and 980 cm^{-1} corresponds to the stretching vibration of Si–O in $[SiO_4]^{4-}$ tetrahedra.[33] The FT-IR spectrum of pure sodium alginate presents asymmetric and symmetric stretching vibrations at 1427 and 1590 cm^{-1} due to carboxyl anions, and that at 1031 cm^{-1} corresponds to oxygen stretching in cyclic ether bridge.[34] The FT-IR spectra of the composite gels, with the AC-4 aerogel as an example, demonstrate that their chemical structure is similar to that of sodium alginate. No significant differences in hydroxyl (–OH) stretching bands at approximately 3400 cm^{-1}, which corresponded to hydroxyl stretching bands in molecular water in Si–OH, are observable. The carboxyl stretching peaks of AC-4 aerogel decreased in intensity and shifted to a higher wavenumber, which may be due to electrostatic interactions between the negative charges of the carboxyl groups and the positively charged sites at the edges of nanoclay. These changes in this peak of alginate were also observed in alginate-bentonite clay composite.[35] These indicate the existence of intermolecular hydrogen bonding and electrostatic forces between alginate and nanoclay. As for the FTIR of nanoclay shifted towards lower wavelengths at around 1000 cm^{-1} compared to the other two materials, it may be other inorganic impurities contained in nanoclay, such as metal oxides or sulfides, whose vibrational modes may contribute to the lower wavelengths at around 1000 cm^{-1} but these impurities are removed during the preparation of the composites.

3.2 Mechanical properties of aerogels

A thermal insulation and flame retarding material needs to have excellent mechanical properties. The compressive properties of various aerogels are tested, and the typical compressive stress–strain curves are shown in Fig. 3a. The nanoclay content affects the compressive strength of an aerogel significantly. When the addition of nanoclay was increased from 0 to 0.40% (AC-3), the AC aerogel exhibited distinct linear elasticity, collapse plateau, and densifications regimes, which is typical for porous aerogels.[36] From the stress–strain curves, the elastic compressive strength (σ_{e1}*) and compressive modulus (E*) can be obtained.[37] The former is determined by linear regression of the

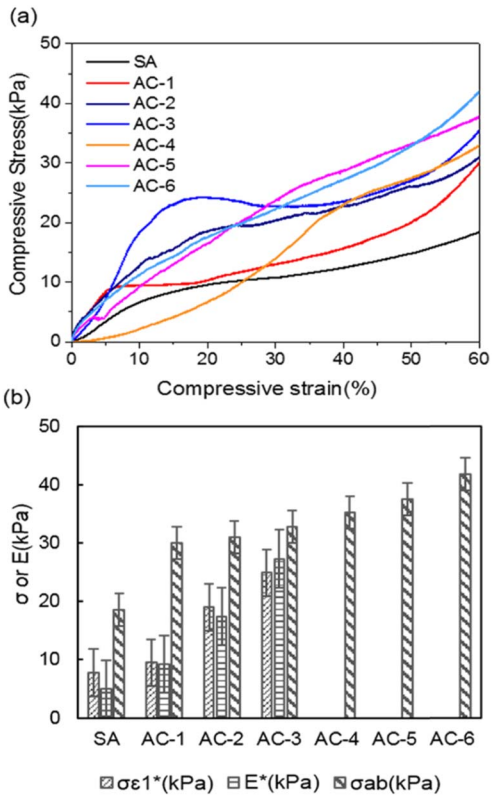

Fig. 3 Effect of the nanoclay addition on the mechanical properties of the alginate aerogel and alginate-nanoclay aerogels. (a) Compressive stress–strain analysis and (b) compressive stress at the maximal strain applied.

initial linear regime of the stress–strain curves and the latter is determined from the intersection of the E^* to Ds/De regression curves. The σ_{e1}* values of SA, AC-1, AC-2 and AC-3 aerogels are 7.8, 9.5, 19.0 and 24.9 KPa, respectively, and their E^* values are 5.0, 9.2, 17.4 and 27.3 KPa, respectively (Fig. 3b). The elastic compressive strength and compressive modulus increase with an increase in nanoclay loading. When the amount of nanoclay was increased to 0.64% (AC-4) and above, the compressive strain–stress curves of the aerogels did not exhibit distinct collapse plateau regime (Fig. 3a). This may be due to the fact that an increased the added amount of nanoclay can easily result in a decrease in its uniform dispersion in the matrix phase, as well as a reduction in the continuity of the matrix phase, which in turn lowers the elastic modulus of the composite material.

Moreover, the compressive strength (σ_{ab}), which is the compressive stress obtained at the maximal compressive strain (*i.e.*, $\sigma_{ab}{}^{0.6}$ 60%,or $\sigma_{ab}{}^{0.8}$ 80%),[38] is increased from 18.5 KPa for the aerogel without nanoclay (SA) to 41.8 KPa for the aerogel with 1.06% nanoclay (AC-6) (Fig. 3b). All the AC aerogels did not collapse even when subjected to a compressive strain of 80%. This enhanced mechanical performance can be attributed to the interfacial/hydrogen bonding between nanoparticles and alginate molecules, as revealed by FT-IR spectra. The nanoclay particles serve as cross-linkers to reinforce the aerogels. Additionally, the typical compressive strain–stress curves of the aerogels could be due to their porous structure as revealed by SEM images and N_2 adsorption/desorption experiment indicated that aerogel exhibits. The disappearance of the distinct collapse plateau regime at high nanoclay contents indicates nanoclay enhances the elasticity of the aerogels.

To investigate the effect of alginate concentration of an aerogel on its mechanical properties, AC aerogels with different alginate concentrations (3% and 4.5%) were prepared while keeping the nanoclay loading constant (0.64%). Results of mechanical testing of these samples are shown in Fig. S1.† All the aerogels show the similar compressive strain–stress curves with linear elasticity, collapse plateau, and densifications regimes. Increasing the concentration of alginate has a positive effect on all the mechanical properties due to increased density of the aerogels. SEM pictures of AC gels with 3% and 4.5% alginate are given in Fig. 1h and i, respectively. Especially, compared with the aerogel with 2% sodium alginate, the compressive strength (σ_{ab}) of the aerogels containing 4.5% of alginate was increased significantly from 35.3 to 163.9 KPa, meanwhile the elastic compressive strength (σ_{e1}*) increased from 7.8 KPa to 24.9 KPa.

To evaluate the mechanical stability and elastic property of AC aerogels, the hysteresis loops were also studied by cyclic tests. The compression stress–strain curves for AC aerogels (AC-4 as an example) at strains of 10%, 20%, 40% and 60% are shown in Fig. 4. The AC-4 aerogel has a stress value of 98.0 KPa at the strain of 10% (Fig. 4a). Increasing the strain to 20%, the stress is increased to 198.8 KPa (Fig. 4b). Both the unloading curves gave a zero stress when compressive strain was removed, obviously without residual strains found under the compressive strains of 10% and 20%, indicating that the aerogel can recover to the original volume. As the strain was increased to 40% (Fig. 4c) and 60% (Fig. 4d), the stress reached 427.9 and 660.4 KPa, respectively, and the samples still did not collapse. Moreover, the residual strains associated with the large strains of 40% and 60% are still very small, indicating the aerogels still maintain good recovery property at these large strains. The hysteresis loop area decreases after the first cycle. The deformation in the first cycle is mainly due to changes in the elastic skeleton of alginate aerogel through mutual contact, collision, and zipping in the alginate networks. After the first cycle, the hysteresis loop area drastically decreased, especially at the strain of 60%. The shrinkage of hysteresis loop area indicates that the related energy dissipation processes are substantially inhibited. The results indicated that as-prepared AC aerogels possess not only excellent elasticity but also super mechanical stability.

Alginate is well-known for its moisture/water absorbing property. Hence, it is interesting and practically significant to understand the effects of moisture content on the mechanical properties of the aerogels. To vary the moisture content, aerogels were exposed to a constant relative humidity (58%) under a constant temperature (20.4 °C) for several days, and then the moisture content and compressive curves were measured by TGA and Instron, respectively. As the compressive strength could be significantly higher at compressive strains above 60% (as can be concluded from Fig. 3a and S1†), the compressive stress–strain curves were measured up to the strain of 80%. Fig. S2a† indicates that the moisture content, determined by weight loss of aerogels at 100 °C, increases from 14.6% to 21.9% when the exposure time is increased from one day to thirty days.

Fig. S2b† shows the influence of moisture on the compressive stress–strain curves. It is obvious that the compressive strength (the compressive stress at the strain of 80%,$\sigma_{ab}{}^{0.8}$) decreased with an increasing moisture content, and the compressive strength exhibits a sharp increase when the strain exceeded 60%. Meanwhile, the elastic mechanical properties are improved with higher moisture contents, as indicated by the extension of the linear elastic regimes. Interestingly, for aerogels having absorbed moisture for 30 days, an elastic mechanical behavior is more obvious. The compressive curve is almost linear in the lower strain range (below 20%). Even after being exposed to moisture for 30 days, the AC aerogels still possessed reasonable mechanical properties.

3.3 Flame retardancy

Butane burner burning tests were used to investigate the fire-resistance of AC aerogels (Fig. 5 and S3†). All samples were exposed to a butane flame with a temperature of 750 °C for several seconds. The flame did not self-propagate and can self-extinguish after the flame was removed from the AC aerogels. Without nanoclay, the aerogel (*i.e.*, SA aerogel) shrinks and its porous structure collapses upon exposure to the flame (Fig. 5). In contrast, the structures of AC aerogels containing nanoclay are less affected. All the aerogel except AC-1 did not break after exposing to the flame. The structure breakdown of AC-1 is due to its lower nanoclay content, which cannot provide sufficient

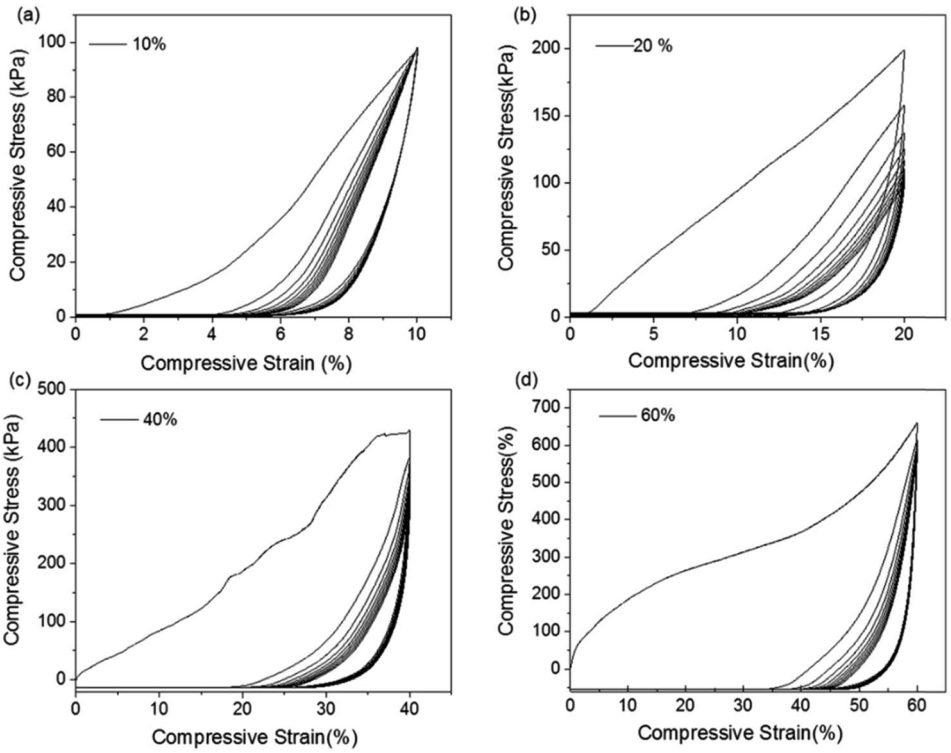

Fig. 4 Compressive stress–strain curves of alginate-nanoclay aerogel up to the measured maximum compressive strain of (a) 10%, (b) 20%, (c) 40% and (d) 60%.

crosslinks. In addition, all the AC aerogels maintained partially or completely their original shapes and porous structures. In terms of structural integrity maintenance, the AC-4 aerogels (loaded with 0.64% nanoclay) showed the best performance, without any obvious change in integrity. More interestingly, it does not give any obvious flame when it was exposed to the butane flame continuously for 20 s, which may contribute to the maintenance of its structural integrity.

To further investigate the flame resistance of aerogels, all the aerogels were exposed to the flame up to 180 s. The corresponding burning times (time that takes an aerogel to collapse when exposed to a flame) were recorded and the residues were calculated (Fig. S3†). Without nanoclay, the SA aerogel collapsed after continuous burning for 15 s and only 20% of its mass was left after burning. It has the shortest burning time and the lowest residue compared with AC aerogels. With the addition of nanoclay, the anti-flame capacity of aerogels was improved in terms of burning time and residue. This could be due to the presence of both nanoclay and Ca^{2+}, which act as flame retardants. Crosslinking of the aerogel by Ca^{2+} and

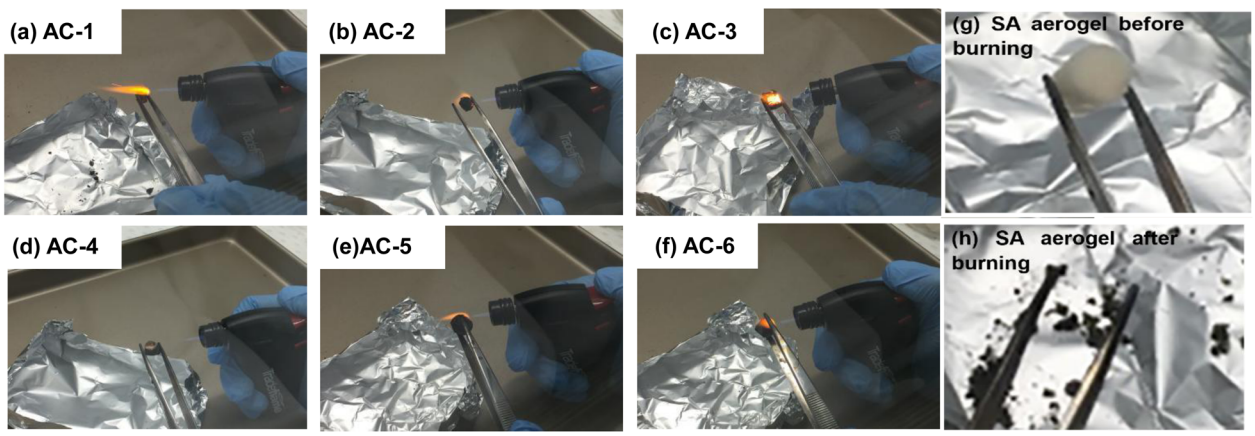

Fig. 5 Photographs taken during butane flame test of different AC aerogels with continuously applying butane flame for 20 s (a–f). AC aerogels retain integrity, while the SA aerogel (g) collapsed after burning (h).

nanoclay could contribute to the flame retardancy of the aerogels. In addition, CaO or $CaCO_3$ generated during samples may also benefit the flame retarding capacity, similarly to other types of inorganic nanoparticles for reducing flammability. Furthermore, Ca^{2+} could provide an alkaline environment for the decarboxylation of alginate and contribute to promote the formation of inert CO_2.[39]

It is interesting to observe in Fig. S3† that AC-4, which has an alginate to nanoclay mass ratio around 3 : 1, demonstrated the best performance. It did not collapse after exposure to the flame for 180 s. It also has highest residue among all the samples. To further understand the flame-retardant behavior of this aerogel, photographs were taken when it was exposed to flame for 10, 60, 120, 180 s and after the flame was removed (181 s) (Fig. 6). The results demonstrated that this aerogel did not release smoke during combustion process, and self-extinguished after being exposed to the flame for 10 s. The reason for the excellent anti-flame capability of this aerogel is unknown. We think that the anti-flame property is contributed by two factors, one of which is the nanoclay content and the other is the porous structure of an aerogel. A higher nanoclay content and a higher porosity shall benefit this property. When an aerogel is exposed to a flame, the pores of an aerogel could absorb moistures and gases such as CO_2 released which inhibits combustion. The SEM images in Fig. 1 demonstrate that AC-5 and AC-6 aerogels have lower porosities, which shall be due to their higher nanoclay contents promoting the nucleation of alginate. Hence, although they have larger nanoclay contents, their anti-flame capacities are lower. The AC-4 aerogel may have the optimal combination of nanoclay content and porosity, contributing to its optimal flame-retardant property.

The thermal properties of SA and AC aerogels (AC-3, AC-4 and AC-5) were investigated by TGA (Fig. S4†). The TGA curve of the SA aerogel is similar to what other researchers reported.[40] Its degradation in Argon proceeds in two-steps: the initial weight loss of SA below 100 °C is attributable to removal of absorbed water. The sharp weight loss around 250 °C should be due to thermal decomposition of SA (Fig. S4a†). On the other hand, in air, SA aerogel usually undergoes a three-step thermo-oxidation. In the first step, from room temperature to 100 °C, the weight loss could be due to the release of absorbed water and the moisture evaporation. In the second step (100–250 °C), the weight loss is due to thermal degradation of alginate. In the third step (250–485 °C), the faster weight loss was attributed to rapid molecular decomposition associated with the fracture of glycosidic bonds, decarboxylation, decarbonylation and dehydration of alginate, releasing CO, CO_2 and other small molecular compounds.[41] The fourth step is situated between 485–650 °C, which shows another shape loss in weight that is due the further thermal degradation of residues from the third stage. The char residual amounts of SA aerogels in air at 500, 600 and 750 °C is 37.9, 34.5, and 32.5% (Fig. S4b†), respectively.

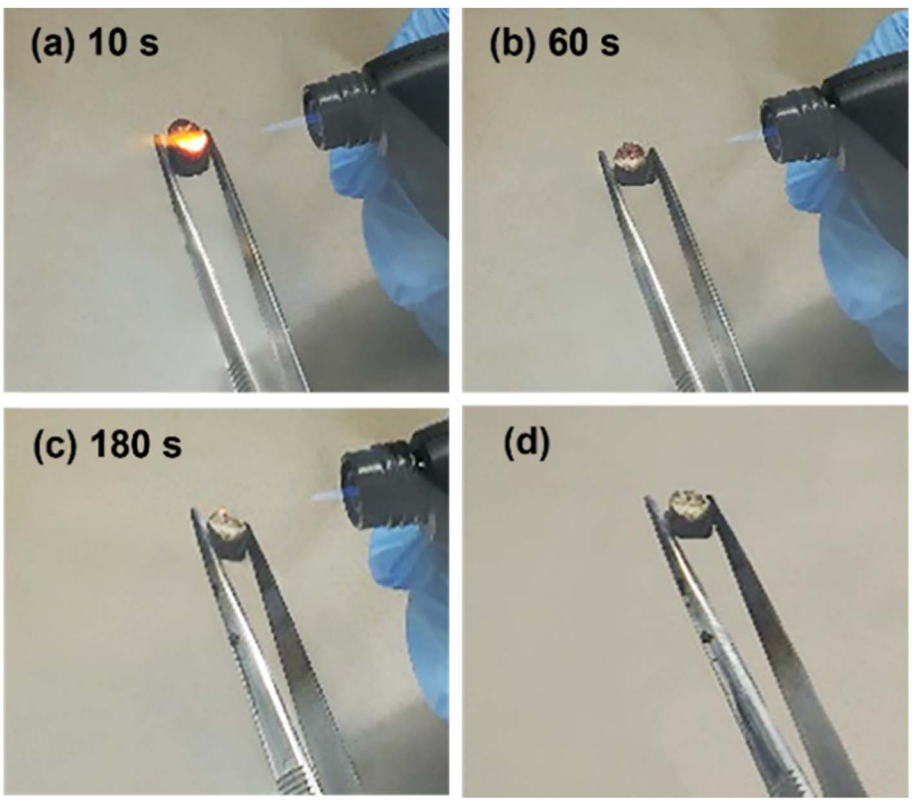

Fig. 6 Photographs taken during butane flame test of the AC-4 aerogel with continuously applying butane flame for different durations. The aerogel did not burn after exposure to the flame for different durations (a–c) and the aerogel maintains its integrity after a long exposure (180 s) of the flame (750 °C) (d).

The aerogels loaded with nanoclay did not affect the thermal and thermo-oxidative degradation temperatures of the aerogels apparently in the second and third step. The presence of nanoclay led to a slight increase in the molecular decomposition temperature of alginate in Argon and a bit more in air, as shown in Fig. S4a and b.† For example, the fourth step decomposition temperature of SA aerogel in air was 485 °C, in contrast, this temperature is 502, 512 and 567 °C for AC-3, AC-4 and AC-5 aerogel, respectively. This indicates nanoclay enhances the thermal stability of alginate. Correspondingly, compared to the SA aerogel, the degradation of AC aerogels has a remarkably higher residue in both argon and air. The char residual amounts of AC-4 aerogels (Fig. S4b†) at 500, 600 and 750 °C were 54.4, 51.2, and 49.3%, respectively, which are significantly higher than that of the SA aerogel.

4 Conclusions

Alginate-nanoclay composite aerogels were fabricated through a facile freezing and post ion crosslinking method. The nanoclay particles, with multiple physical interactions with alginate molecules, served as additional cross-linkers to improve the mechanical strength, elasticity, and flexibility of the aerogels. The composite aerogels exhibited excellent flame resistance and burned with low flammability and little or no residual char. Interestingly, a loading of nanoclay which led to optimal flame retardancy was observed. In addition, the aerogels self-extinguish when flame is removed, and no drips can be resulted. All these performances indicate the nanoclay-reinforced alginate aerogels are excellent flame retarding materials.

Data availability

The raw/processed data required to reproduce these findings cannot be shared at this time as the data also forms part of an ongoing study.

Conflicts of interest

There are no conflicts to declare.

Acknowledgements

YL Tai acknowledges supports from Zhejiang Province Health Commission Research Foundation of China (2024ZL370, 2024KY918).BT Xu acknowledges supports from National Innovation and Entrepreneurship Training Program for College Students (202313023018), Science and Technological Innovation Project for College Students in Zhejiang Province (Xinmiao Talent Plan 2020R425003) and Innovation and Entrepreneurship Elite Project of Hangzhou Medical College's Humanity Entrepreneurship Education Fund. Y Yi acknowledges supports from Innovation and Entrepreneurship Training Program for College Students of Zhejiang Province (S202313023082). Special Health Program of Zhejiang Province (Grant No. YS2022008).

References

1 O. Das, N. K. Kim, A. K. Sarmah and D. Bhattacharyya, *J. Cleaner Prod.*, 2017, **144**, 79–89.
2 M. Palumbo, J. Formosa and A. Lacasta, *Constr. Build. Mater.*, 2015, **79**, 34–39.
3 S. T. McKenna and T. R. Hull, *Fire Sci. Rev.*, 2016, **5**, 1–27.
4 M.-H. Son, Y. Kim, Y.-H. Jo and M. Kwon, *Forensic Sci. Int.*, 2021, **328**, 111011.
5 P. Xiong, X. Yan, Q. Zhu, G. Qu, J. Shi, C. Liao and G. Jiang, *Environ. Sci. Technol.*, 2019, **53**, 13551–13569.
6 G. Vahidi, D. S. Bajwa, J. Shojaeiarani, N. Stark and A. Darabi, *J. Appl. Polym. Sci.*, 2021, **138**, 50050.
7 Z. Kovačević, S. Flinčec Grgac and S. Bischof, *Polymers*, 2021, **13**, 741.
8 R. Nishita, K. Kuroda, S. Ota, T. Endo, S. Suzuki, K. Ninomiya and K. Takahashi, *New J. Chem.*, 2019, **43**, 2057–2064.
9 Y.-J. Xu, L.-Y. Qu, Y. Liu and P. Zhu, *Carbohydr. Polym.*, 2021, **260**, 117827.
10 N. Blanco-Pascual, M. Montero and M. Gómez-Guillén, *Food Hydrocolloids*, 2014, **37**, 100–110.
11 M. Hemath, S. Mavinkere Rangappa, V. Kushvaha, H. N. Dhakal and S. Siengchin, *Polym. Compos.*, 2020, **41**, 3940–3965.
12 L. M. Llive, M. Perullini, P. R. Santagapita, A. Schneider-Teixeira and L. Deladino, *Eur. Polym. J.*, 2020, **138**, 109955.
13 S. D. Rekha and B. Trinath, *SN Appl. Sci.*, 2021, **3**, 30.
14 A. Lisette, A. Saadet, I. Elif, Z.-S. Dionisio and G. Oguzhan, *Eur. Polym. J.*, 2021, 160.
15 O. Connie, D. Sorina, S. Iuliana, D. G. Cristina, C. Andreia, C. Marizeta and A. Luc, *Eur. Polym. J.*, 2021, 110444.
16 M. Cibinel, G. Pugliese, D. Porrelli, L. Marsich and V. Lughi, *Carbohydr. Polym.*, 2021, 251.
17 J. Liu and C. Xiao, *Int. J. Biol. Macromol.*, 2018, **119**, 1083–1089.
18 K. Vilcinskas, K. M. B. Jansen, F. M. Mulder, S. J. Picken and G. J. M. Koper, *Polym. Compos.*, 2018, **39**, E236–E249.
19 B. K. Basavarajappa, R. N. Marulaiah and R. J. Sundara, *Polym. Compos.*, 2021, 42.
20 K. Hu, D. D. Kulkarni, I. Choi and V. V. Tsukruk, *Prog. Polym. Sci.*, 2014, **39**, 1934–1972.
21 D. Junjie, Z. Hong, W. Wenbo, Z. Yongfeng, W. Qin and W. Aiqin, *Eur. Polym. J.*, 2021, 147.
22 Z. Shuai, D. Chunxiang, H. Yanping and P. Mingzhu, *Polym. Compos.*, 2021, 42.
23 J. W. Gilman, *Appl. Clay Sci.*, 1999, **15**, 31–49.
24 H.-B. Chen and D. A. Schiraldi, *Polym. Rev.*, 2019, **59**, 6790–6796.
25 W. S. Tan and A. S. Y. Ting, *Bioresour. Technol.*, 2014, 160.
26 S. Leporatti, *Polymers*, 2019, 11.
27 A. Mazumder, S. L. Holdt, D. D. Francisci, M. Alvarado-Morales, H. N. Mishra and I. Angelidaki, *J. Appl. Phycol.*, 2016, **28**, 3625–3634.
28 F. Linpeng, L. Jing-Liang, C. Zengxiao and W. Xungai, *ACS Nano*, 2018, **12**, 5780–5790.

29 G. Shao, D. A. Hanaor, X. Shen and A. Gurlo, *Adv. Mater.*, 2020, **32**, 1907176.
30 J.-L. Li, B. Yuan, X.-Y. Liu, R.-Y. Wang and X.-G. Wang, *Soft Matter*, 2013, **9**, 435–442.
31 J. L. Li and X. Y. Liu, *Adv. Funct. Mater.*, 2010, **20**, 3196–3216.
32 A. A. Edathil, P. Pal and F. Banat, *Appl. Clay Sci.*, 2018, 156.
33 R. L. Frost, J. Čejka, M. L. Weier and W. Martens, *J. Raman Spectrosc.*, 2006, **37**, 538–551.
34 J. Kloprogge, *Spectroscopic Methods in the Study of Kaolin Minerals and Their Modifications*, Springer, Cham, pp. 161–241.
35 A. Benhouria, M. A. Islam, H. Zaghouane-Boudiaf, M. Boutahala and B. H. Hameed, *Chem. Eng. J.*, 2015, 270.
36 G. Xiong, H. Luo, G. Zuo, K. Ren and Y. Wan, *Mater. Charact.*, 2015, **107**, 798–805.
37 G. Weiwei, Z. Nifang, Y. Weiquan, X. Zhen, B. Hao and G. Chao, *RSC Adv.*, 2017, **7**, 33600–33605.
38 C. Jiao, J. Xiong, J. Tao, S. Xu, D. Zhang, H. Lin and Y. Chen, *Int. J. Biol. Macromol.*, 2016, **83**, 133–141.
39 J. Zhang, Q. Ji, F. Wang, L. Tan and Y. Xia, *Polym. Degrad. Stab.*, 2012, **97**, 115693.
40 N. Işıklan and Z. Altınışık, *J. Appl. Polym. Sci.*, 2018, **135**, 352–362.
41 H.-B. Chen, Y.-Z. Wang, M. Sánchez-Soto and D. A. Schiraldi, *Polymer*, 2012, **53**, 5825–5831.